Electronic Supplementary Information for

Chemically functionalized 3D graphene hydrogel for high performance gas sensing

Jin Wu, [a] Kai Tao, [a] Jing Zhang, [d] Yuanyuan Guo, [d] Jianmin Miao *[a] and Leslie K. Norford [bc]

[a]School of Mechanical and Aerospace Engineering, Nanyang Technological University, Singapore 639798, Singapore

[b]Center for Environmental Sensing and Modeling (CENSAM), Singapore-MIT Alliance for Research and Technology (SMART) Centre, Singapore 117543, Singapore

[c]Department of Architecture, Massachusetts Institute of Technology, Cambridge, MA 02139, USA

[d]School of Materials Science and Engineering, Nanyang Technological University, 50 Nanyang Avenue, Singapore 639798, Singapore

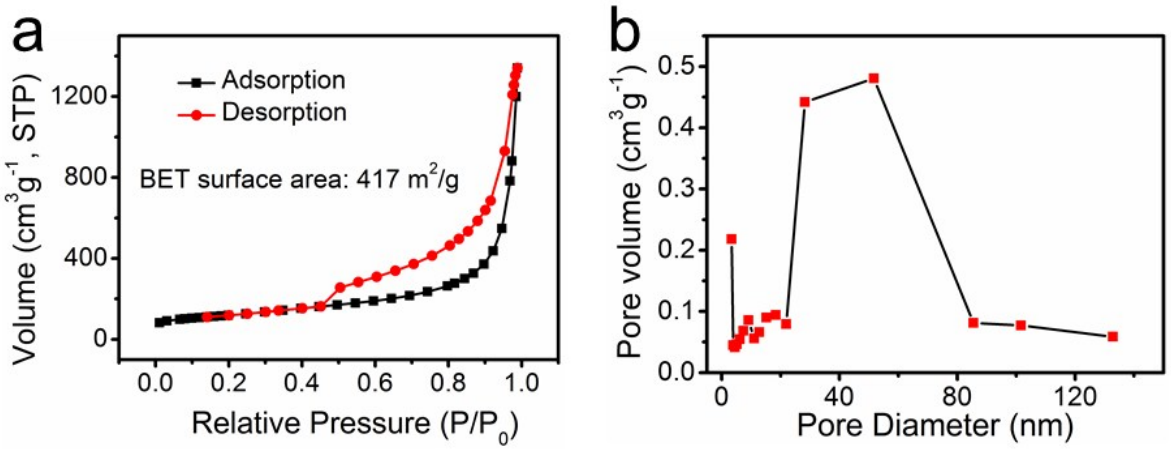

Figure S1 (a) Nitrogen adsorption and desorption isotherms of the freeze-dried FRGOH. (b) BJH pore distribution of the freeze-dried FRGOH.

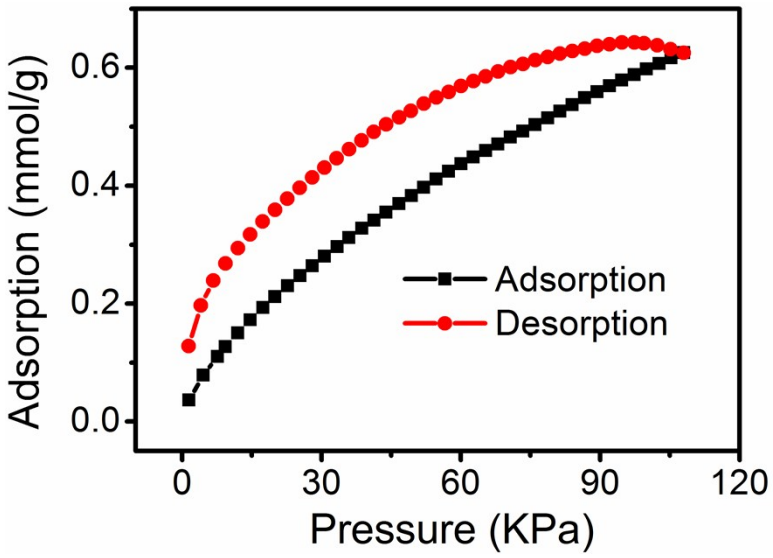

Figure S2 CO_2 adsorption-desorption isotherms of FRGOH.

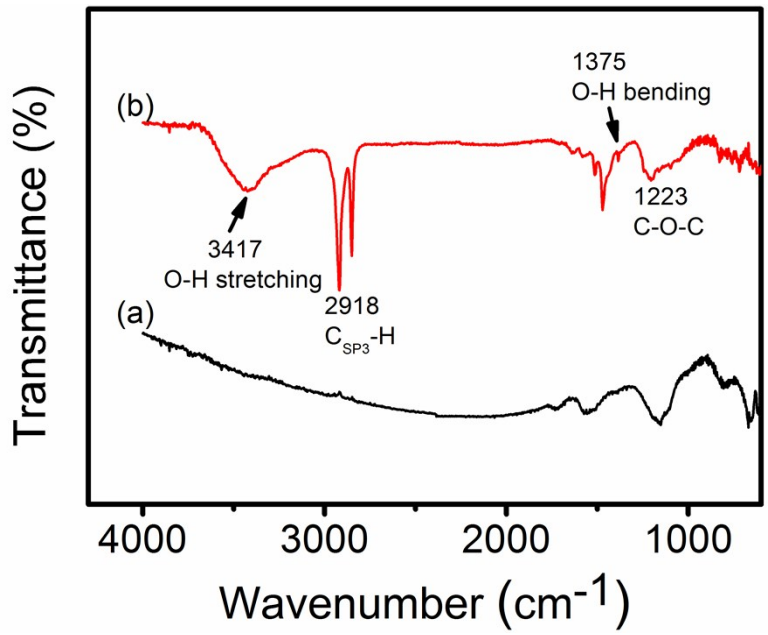

Figure S3 FTIR spectra of (a) as-prepared 3D RGOH and (b) FRGOH.

a

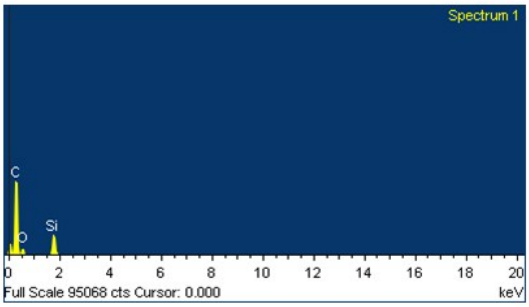

Element	Weight%	Atomic%
C K	79.02	84.69
O K	16.43	13.22
Si K	4.55	2.09
Totals	100.00	

C/O= 6.41

b

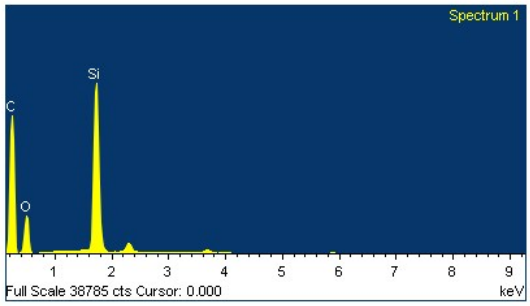

Element	Weight%	Atomic%
C K	65.28	74.26
O K	24.06	20.55
Si K	10.66	5.19
Totals	100.00	

C/O= 3.61

Figure S4 Energy-dispersive X-ray (EDX) spectra of the RGOH (a) and FRGOH (b). The ratio of C to O in RGOH (6.41) was much higher than that in FRGOH (3.61). The increased percentage of oxygen in FRGOH compared to that in RGOH was attributed to the successful

modification of hydroquinone molecules on FRGOH surface. The Si signal comes from the silicon substrate.

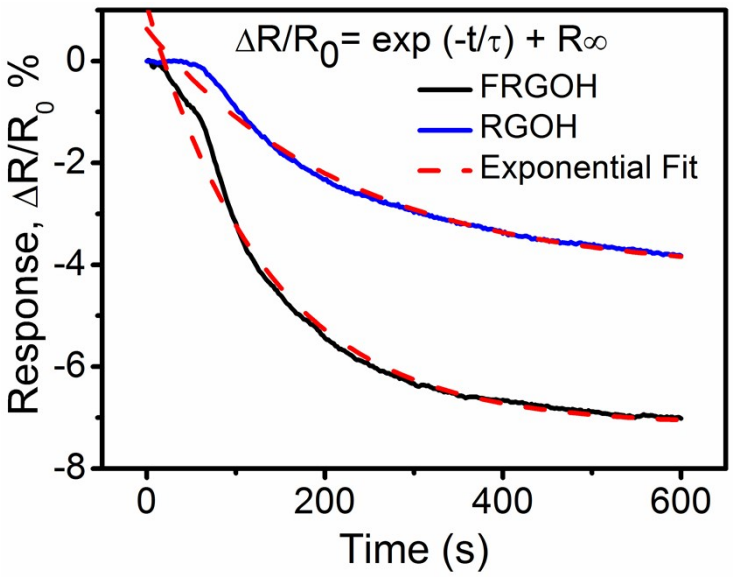

Figure S5 Exponential fitted responses of the FRGOH and RGOH sensors to 10 ppm NO_2 versus time curves at 22 °C. The time constants for the FRGOH and RGOH sensors were calculated to be 143 and 222 s, respectively, from the fitted curves.

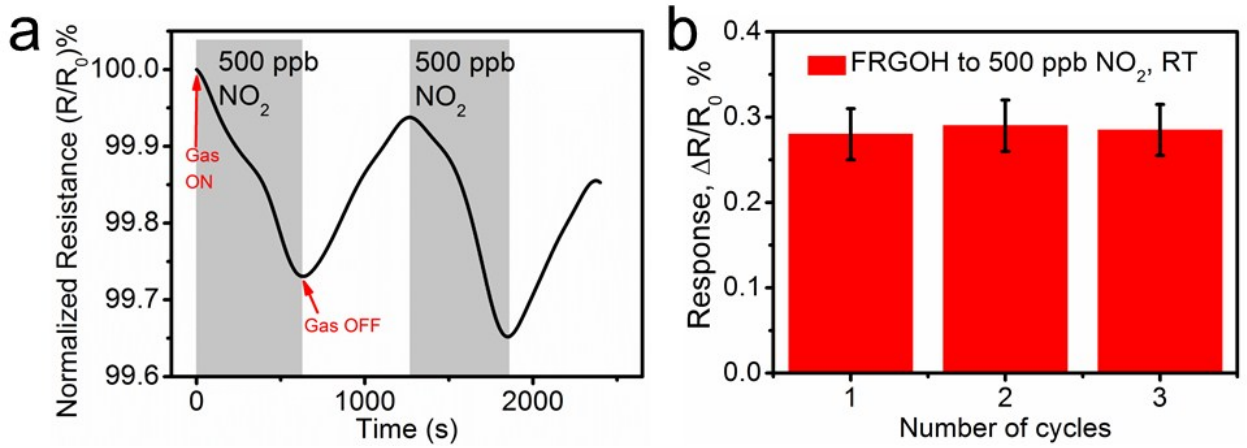

Figure S6 Investigation of the repeatability of the FRGOH sensor by detecting 500 ppb NO_2 gas repeatedly. a) Normalized resistance of the sensor versus time upon exposure to 500 ppb NO_2

repeatedly in selected two cycles. b) The response of the FRGOH sensor to 500 ppb NO_2 for three consecutive cycles.

Calculation of sensitivity, noise level (RMS_{Noise}) and LOD of the FRGOH and RGOH based NO_2 sensors.[S1,S2]

1. Execute linear fitting of the response versus NO_2 concentration curve in the linear region, followed by obtaining the slope (sensitivity) and standard error from the fitted line (Figure S7a and c).

2. Perform polynomial fit (5^{th} order) for response $\Delta R/R$ versus time (sec) curves at the baseline before NO_2 exposure (Figure S7b and d).

3. Take 10 data points at the baseline before NO_2 exposure (Y_i).

4. Calculate regular residual (Y_i-Y) and statistical parameters of 5^{th} order polynomial fit, in which Y_i is the measured data point and Y is the corresponding value calculated from the fitted curve (Table S1-2).

5. Calculate the root-mean squared deviation (RMS_{Noise}) and LOD using Equation S1 and S2 (Table S3).

RMS_{Noise} (ppm^{-1}) = $\sqrt{(V_x^2/(N-1))}$, where $V_x^2 = \sum(Y_i-Y)^2$ (Equation S1)

LOD (ppm) = 3 × RMS_{Noise} / Slope (Equation S2)

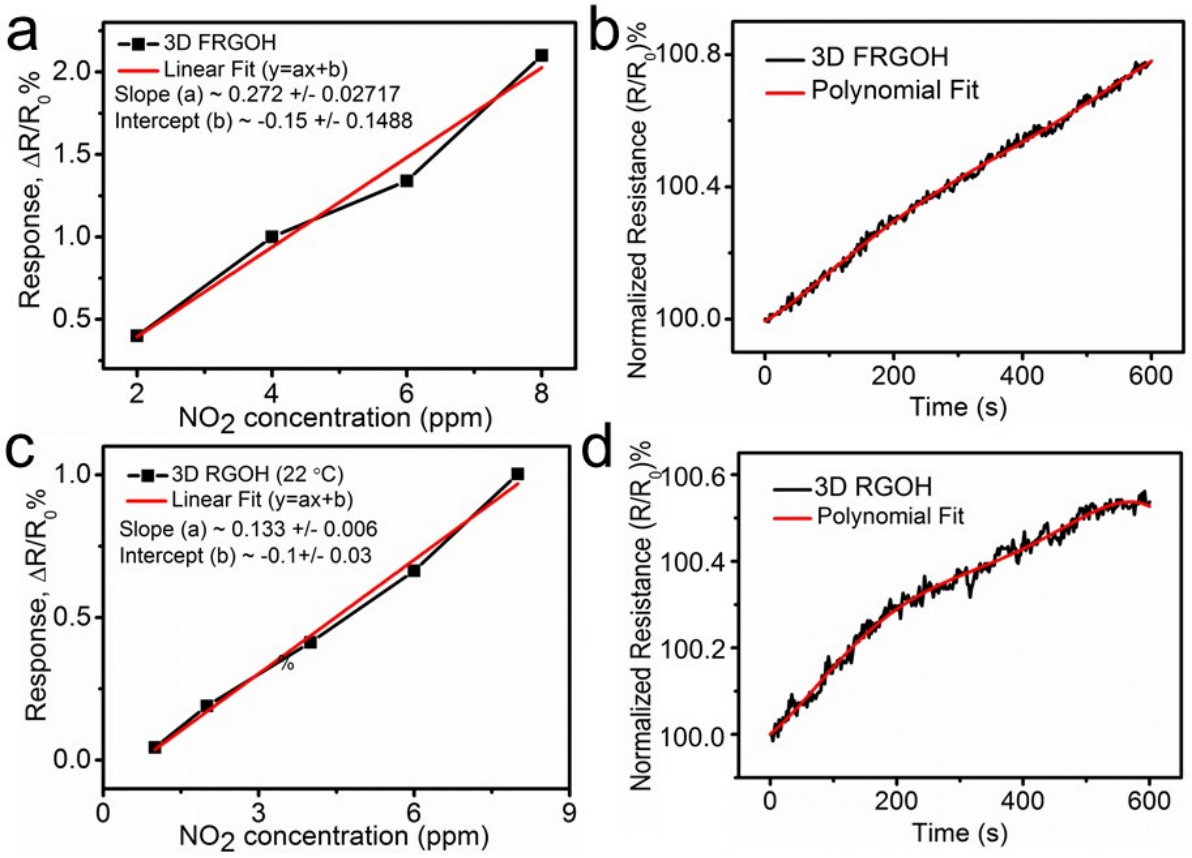

Figure S7 a) and c) The experimentally obtained response (dashed black line) and linear fitted response (red line) as a function of NO_2 concentration for the 3D FRGOH and RGOH sensors respectively. b) and d) Plots of 5th order polynomial fitted normalized resistance of the 3D FRGOH and RGOH sensors respectively as a function of time at the baseline before NO_2 exposure.

Table S1 5th order polynomial fitting data for 3D FRGOH sensor

Time (sec)	Y_i-Y	$(Y_i-Y)^2$
0	5.9921E-3	3.59E-05
50	7.17865E-4	5.15E-7
100	3.25829E-3	1.06E-05
150	0.011	1.21E-04
200	4.46791E-3	2.00E-05
250	2.14109E-3	4.58E-06
300	4.04534E-3	1.64E-05
350	3.51092E-3	1.23E-05
400	2.65748E-3	7.06E-06
450	-5.3288E-3	2.84E-05
500	-3.82043E-3	1.46E-05

Table S2 5th order polynomial fitting data for 3D RGOH sensor

Time (sec)	Y_i-Y	$(Y_i-Y)^2$
0	-8.81E-03	7.76E-05
50	-4.75E-03	2.26E-05
100	1.62E-03	2.62E-06
150	-3.50E-03	1.23E-05
200	-1.77E-03	3.13E-06
250	8.22E-03	6.76E-05
300	4.18E-03	1.75E-05
350	-1.24E-03	1.54E-06
400	1.03E-02	1.06E-04
450	-2.96E-03	8.76E-06
500	2.15E-02	3.06E-04

Table S3 Calculation of sensitivity, RMS $_{noise}$ and LOD

Material for NO_2 Sensing	Slope (Sensitivity) (ppm^{-1})	Standard Error (ppm^{-1})	V_x^2	RMS_{noise}	LOD (ppm)
3D FRGOH	0.272	0.0272	0.000271	0.00521	0.057
3D RGOH	0.133	0.006	0.000626	0.00791	0.178

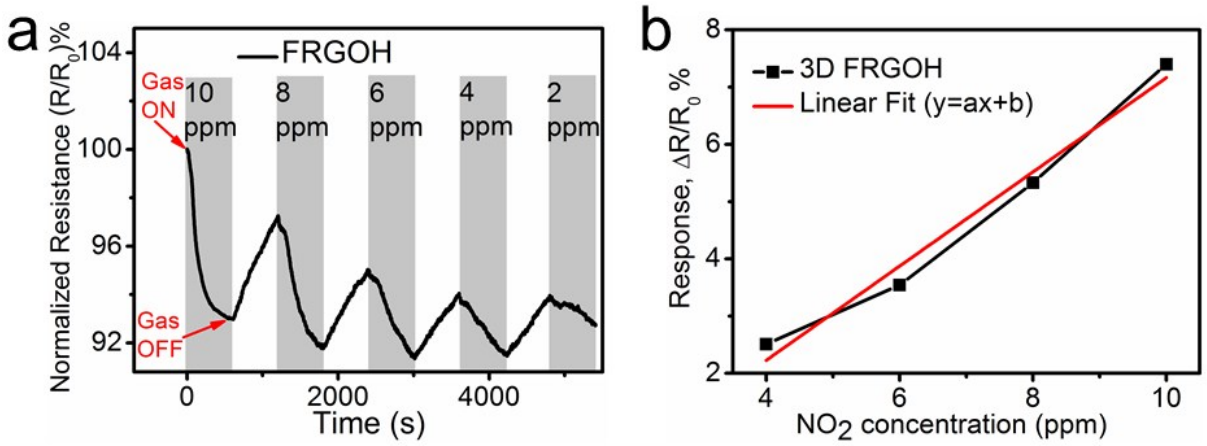

Figure S8 NO_2 sensing with nearly linearly decreased response with NO_2 concentration. a) Normalized resistance change of the FRGOH sensor upon exposure to NO_2 with linearly reduced concentration. b) The measured and linearly fitted response of the FRGOH sensor versus NO_2 concentration in (a). In this experiment, the gas chamber was opened in the air purge process after stopping NO_2 exposure. As such, the NO_2 molecules adsorbed on FRGOH surface can be expelled more completely in the air purge process. After air purge, the gas chamber was closed

again for the next reversible NO_2 test cycle. It was found that the response changed nearly linearly with NO_2 concentration after stabilizing the sensor before the next reversible sensing in this manner.

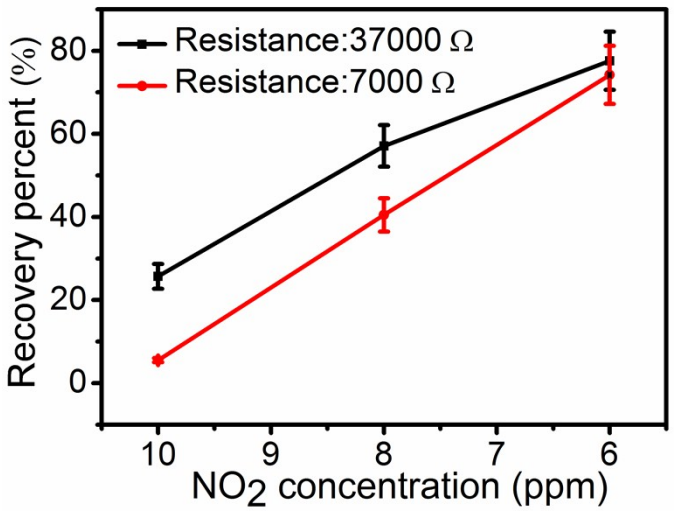

Figure S9 Comparison of the recovery percentage between the FRGOH sensor with the resistance of 37000 Ω and that with the resistance of 7000 Ω in NO_2 sensing.

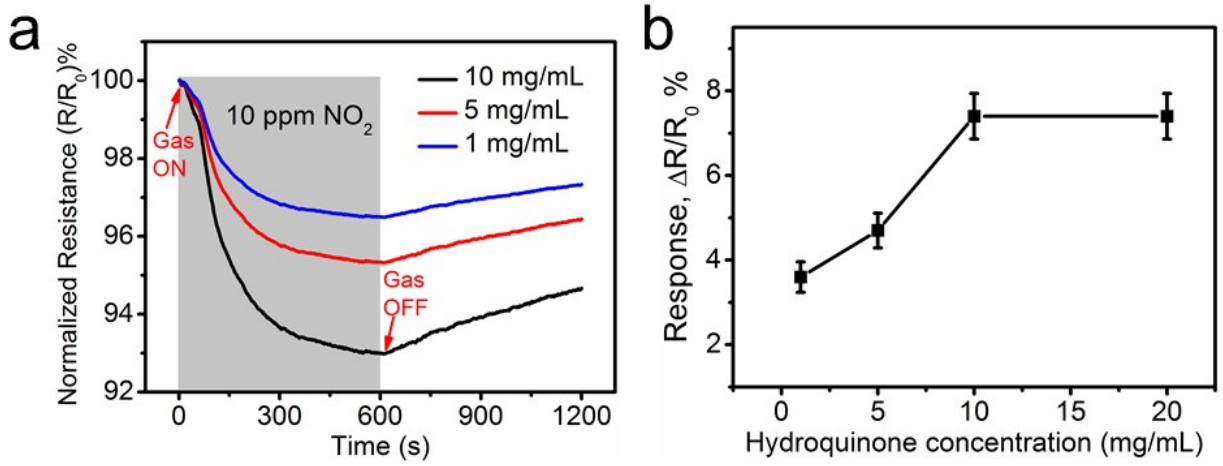

Figure S10 The effect of the content of hydroquinone component on the sensitivity of NO_2 detection. a) Comparison of normalized resistance versus time curves for FRGOH that

synthesized from hydroquinone aqueous solution with the concentrations of 10, 5 and 1 mg/mL respectively in 10 ppm NO_2 sensing. b) Response of the sensor to 10 ppm NO_2 as a function of hydroquinone concentration.

Fabrication of microheater

The microheater was fabricated on one side of a Si/SiO_2 wafer by microfabrication and micromachining technologies.[S3] In order to make the serpentine Pt lines dominate the heat generation, the microheater was designed with the Pt line width of 30 μm and the contact pad size of 1×1 mm^2. After spin-coating of a 5 μm thick AZ 9260 photoresist layer on Si/SiO_2 wafer, traditional photolithography was performed with a mask aligner, followed by sputtering of 10 nm Ti/300 nm Pt and lifting off the photoresist to pattern platinum (Pt) heating lines onto the substrate. Another photolithography, metal deposition and lift off process were employed to pattern gold contacting pads (300 nm thick) in the same manner. Due to the Joule effect, the microheater heated the sensor to the desired temperature quickly when a direct current (DC) power supply was deployed to apply a DC voltage on the microheater.[S3] An infrared camera (TYPE F30W, NEC Avio Infrared Technologies Co., Ltd) was deployed to measure the temperature of microheater and collect the optical image that showing temperature distribution on substrate.

Characterization of microheater

The resistance of a microheater can be determined by $R = \rho l/(dw)$, where R, ρ, l, d and w are resistance, electrical resistivity, length, thickness and width of the resistor respectively. When a DC voltage is applied on the electrodes of the microheater, the serpentine Pt lines heat the Si/SiO_2 wafer due to the Joule effect with the power of $P = U^2/R$. In order to make the 30 μm

wide serpentine Pt lines shown in Figure 4a generate most of heat, the electrical wirings and contact pads are much wider (e.g., the Au contact pads have the size of 1×1 mm^2). Because of the low thermal conductivity of the SiO_2 layer (~1 $Wm^{-1}K^{-1}$) on the Si substrate, the temperature of the region with the Pt lines is much higher than that at other parts of the substrate. [S3]

Figure 4c showed that the current and the average temperature of the microheater increased monotonically with increased voltage. For example, the temperature of the substrate was 22, 38 and 79 °C when the DC voltages of 0, 5 and 10 V were applied on the microheater respectively. The slope of the current-voltage (I-V) curve reduces gradually owning to increased resistance of the microheater at elevated temperature. The temperature-resistance relationship of a microheater can be expressed by this following equation:

$$R = R_0[1+\alpha(T-T_0)] = (R_0-\alpha R_0 T_0) + \alpha R_0 T \qquad \text{(Equation S3)}$$

in which R_0 is the resistance at the reference temperature T_0 =20 °C and α is the temperature coefficient of resistance (TCR) of the resistor.[S3] From the experimentally obtained temperature-resistance relationship (dash-dot black line in Figure S11), the curve can be linearly fitted as $R = 0.30613T+70.124$. To make a comparison between this equation with equation S3, we can obtain: $R_0-\alpha R_0 T_0=70.124$ and $\alpha R_0=0.30613$. Thus, the TCR can be calculated to be $\alpha \approx 0.004$ $°C^{-1}$, which approaches that of pure Pt ($\alpha \approx 0.0039$ $°C^{-1}$).[S3] Hence, the temperature of substrate and sensing material can be conveniently controlled and monitored by using the applied DC voltage (Figure 4c). For example, the optical image of the substrate captured by the infrared camera (TYPE F30W, NEC Avio Infrared Technologies Co., Ltd) showed that the substrate was heated to 38 °C when the DC voltage of 5 V was applied to the microheater (Figure 4b).

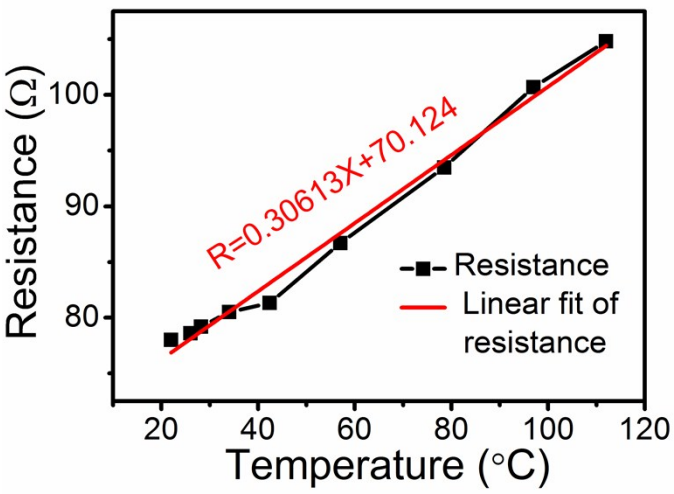

Figure S11 The experimentally obtained (dash-dot black line) and linearly fitted (straight red line) resistance versus temperature curves of the microheater.

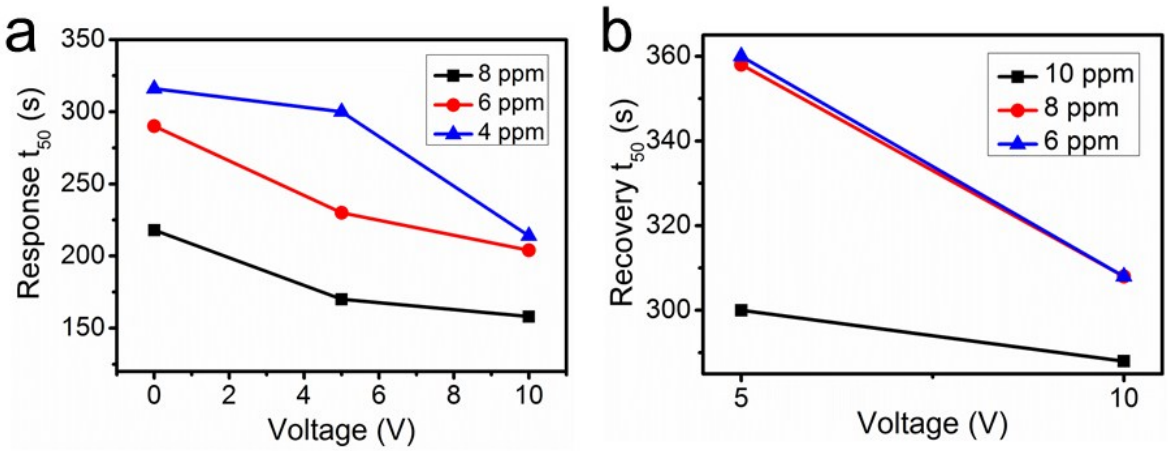

Figure S12 a) and b) Response and recovery time (t_{50}) analysis of the FRGOH based NO_2 sensor as a function of DC voltage applied to the microheater.

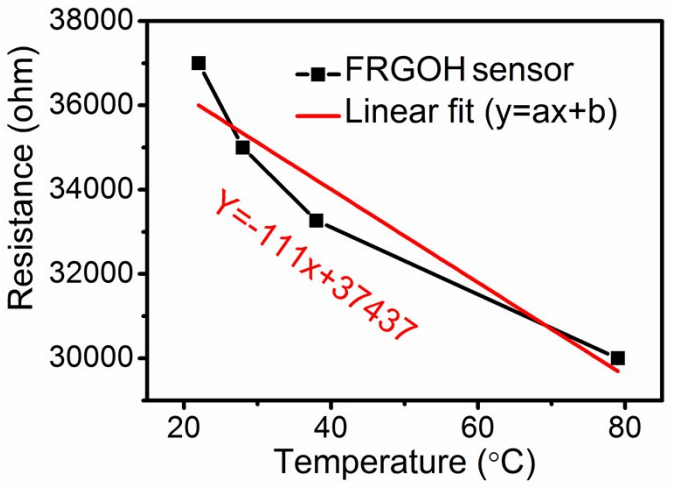

Figure S13 The experimentally measured (black dash-dot line) and linearly fitted (red straight line) resistance of the FRGOH sensor as a function of temperature.

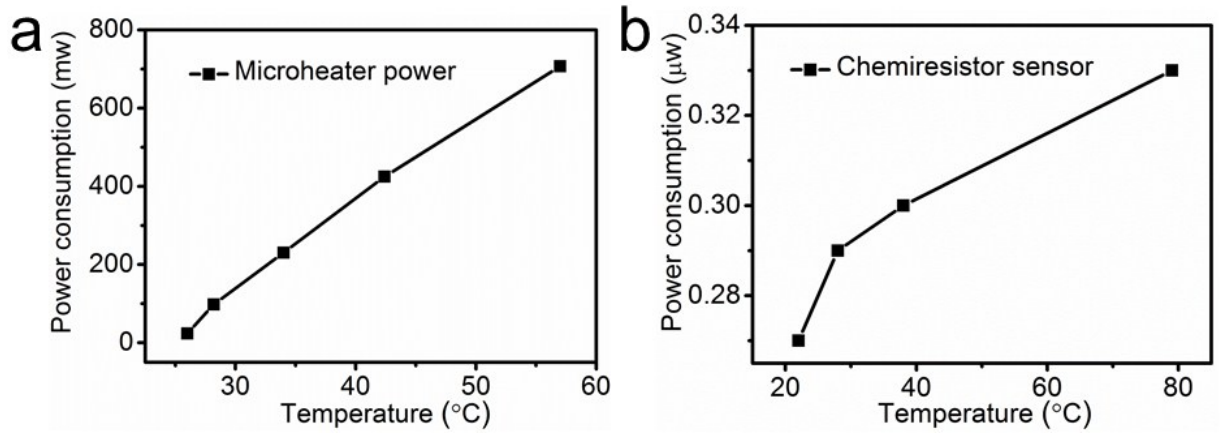

Figure S14 a) and b) The power consumption of the microheater and chemiresistor sensor as a function of the substrate temperature respectively.

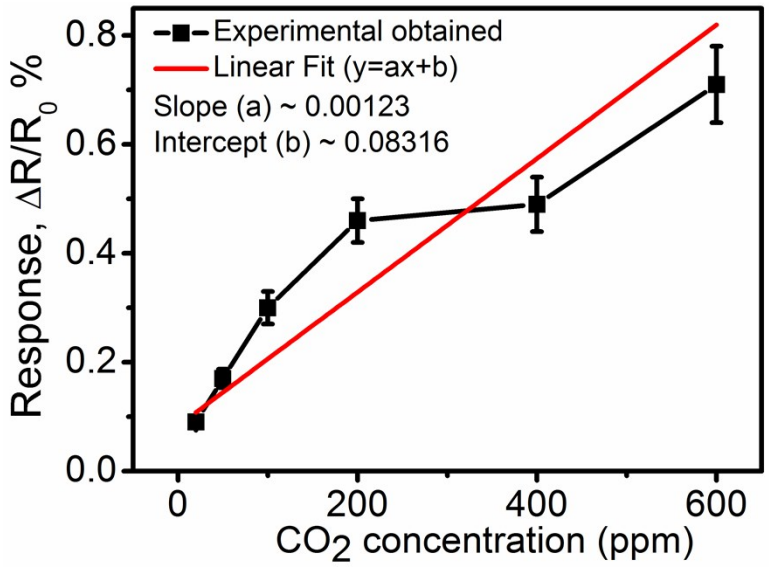

Figure S15 Monotonically increased response of the FRGOH sensor to CO_2 with the increased concentration from 20 to 600 ppm.

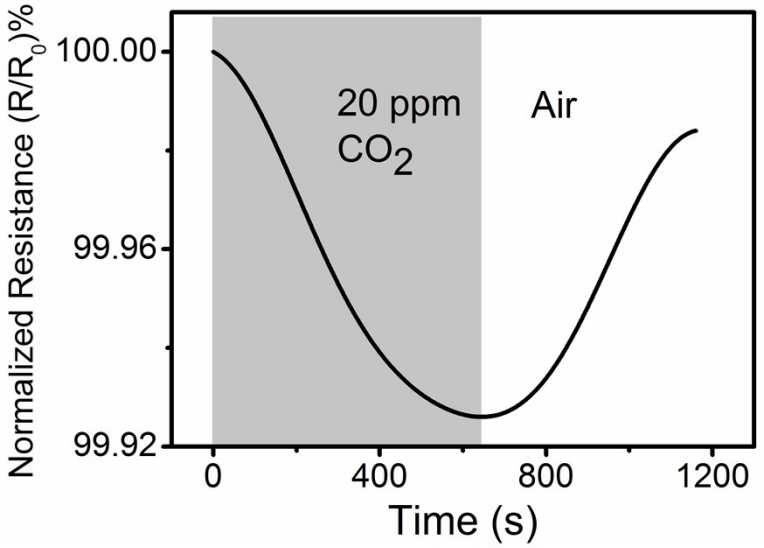

Figure S16 Response of the FRGOH sensor to 20 ppm CO_2.

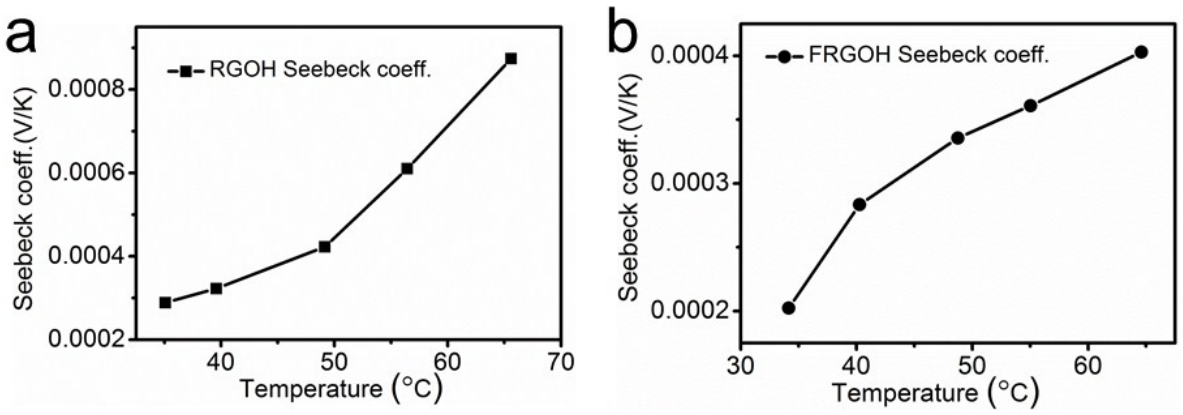

Figure S17 Plots of the measured Seebeck coefficient of RGOH (a) and FRGOH (b) from 35 to 65 °C by ULVAC ZEM-3.

References

1 L. T. Duy, D.-J. Kim, T. Q. Trung, V. Q. Dang, B.-Y. Kim, H. K. Moon and N.-E. Lee, *Adv. Funct. Mater.*, 2015, **25**, 883.

2 V. Dua, S. P. Surwade, S. Ammu, S. R. Agnihotra, S. Jain, K. E. Roberts, S. Park, R. S. Ruoff, S. K. Manohar, *Angew. Chem. Int. Ed.* 2010, **49**, 2154.

3 J. Y. Lu, J. M. Miao, L. K. Norford, *Carbon* 2013, **57**, 259.